VIRTUAL MEDICAL IMAGING FROM TEXTURE SYNTHESIS

PRIETO Juan-Carlos ⋆ *REVOL-MULLER Chantal* ⋆ *PEYRIN Françoise* ⋆† *ODET Christophe* ⋆

⋆ CREATIS, INSA, 7 Avenue Jean Capelle 69621, Lyon, France
† ESRF, BP 220, 38043 Grenoble Cedex, France

ABSTRACT

Image simulation software is essential to improve medical image acquisition devices, segmentation and reconstruction algorithms, and to provide low cost datasets for research purposes. Since the simulated image is derived from a digital model, it provides a gold standard to compare the output of these methods. We present a method based on texture synthesis, able to produce 3D medical images from 2D textured samples. The method is based on a distance metric that compares neighborhoods in the 2D reference sample and the 3D generated object. After an optimization driven by an energy minimization, the result is a solid object that resembles the sample at every slice. We apply our method to synthesize virtual medical images from 2D slices extracted from SRμCT and μMR images. We demonstrate the accuracy of the generated texture by comparing statistical and morphological parameters computed from the virtual images with those obtained from the real images.

Index Terms— Image simulation, Medical images, texture synthesis, virtual human

1. INTRODUCTION

Medical imaging consists in acquiring details of the interior of the human body by using different techniques. Among these techniques we find MRI (magnetic resonance imaging), CT (computed tomography), US (ultra sounds) or PET (positron emission tomography). They are widely used to diagnose, plan and treat patients with the information acquired in the image. Nowadays, it is desired to achieve higher resolution levels in the acquisitions, therefore experimental imaging such as $\mu MRI, \mu CT$ or $SR\mu CT$ (Synchrotron Radiation X-Rays Computed Micro-Tomography) are still evolving. Unfortunately, they are not used in vivo because of problems related to dose radiation. $SR\mu CT$ is able to produce images up to 0.28 μm, presenting unique characteristics in terms of spatial density resolution and signal to noise ratio. Consequently, it is the reference tool to investigate the micro structure of bone samples [**?**].

These kinds of experimental imaging devices are very expensive, they require regular maintenance and are used only by specialized staff. The produced data is very limited since in some occasions is private, thus making it unavailable to other research purposes, or the acquisition protocols are performed sparingly. Image simulation is an alternative to produce low cost datasets of an image modality. There are two basic approaches. The first one consists in applying the physics present in the acquisition process to a digital model [**?**]. The digital model can be used afterwards to validate and improve segmentation or quantification algorithms. The second approach is related to texture synthesis, it was intended to mimic mammograms [**?**] or to designing scaffolds based on the bone micro structure [**?**].

In this paper, we propose a method related to the second approach, which is generic enough to reproduce 3D μMR and $SR\mu CT$ images. The texture synthesis algorithm is similar to the one proposed by Kopf [**?**], it starts with a 2D reference texture provided by slices extracted from a μMR or $SR\mu CT$ acquisition and by means of an energy optimization process described by Kwatra [**?**], the method is able to create a 3D texture that resembles the 2D image in every slice.

The texture synthesis optimization has the advantage of creating models, using one or multiple samples to constrain the view perpendicular to each axis direction, extra channels can be added to the exemplar, like distance maps which are useful to code large textured features [**?**]. The method also maintains the global statistics of the sample by using a histogram matching approach [**?**]. The following section describes our method to synthesize realistic 3D virtual images from slices of μMR, $SR\mu CT$ acquisitions. In section 3, we present the generated virtual images. The accuracy of the synthetic images is assessed and discussed by comparing statistical and morphological parameters computed from the virtual and the real images.

2. METHOD

2.1. 3D Texture Synthesis

Our approach is based on an energy function proposed by [**?**] and defined by the following equation:

$$E(o, \{e\}) = \sum_{t} \sum_{i \in \{x,y,z\}} ||o_{t,i} - e_{t,i}||^r \qquad (1)$$

It is based on a distance metric that compares the neighborhoods x, y, z of a texel t in the object o and neighborhoods from the sample texture e. When minimized, using IRLS (iterative re-weighted least squares), the result is an increase of similarity between the sample and the synthetic object. The procedure begins at a coarse resolution assigning random values from the sample to the synthetic object. Then, it alternates between a search phase where the closest neighborhoods are found and an optimization phase where the weighted average of every texel is calculated. When the optimization converges, it changes to a finer resolution level using linear interpolation.

2.1.1. Search phase

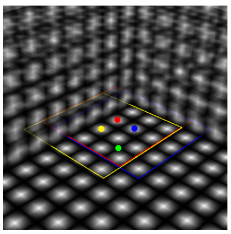

Fig. 1. Different neighborhoods and their center pixel (red, yellow, blue) shown in a slice of the volume, one pixel (green) is affected by multiple neighborhoods

The sample image is divided into $9*9$ neighborhoods that overlap each other, these neighborhoods are vectorized *i.e.* every texel from the neighborhood is stacked into a single vector. For RGB texels we have $9*9*3 = 243$ values in a single vector. It is possible to use a distance map as an extra channel by giving the algorithm a binary image as input, this is useful when the texture has large unstructured areas. Once the vectors from the sample are constructed, we apply PCA (principal component analysis) [1] to reduce the dimensionality of each vector passing from 243 to 18 values approximately. Reducing the vectors is a very convenient step, there are less values but we are still keeping 95% of the relevant information. The reduced vectors can be used to perform a standard closest neighborhood search in a high dimensional space. For this purpose, we use ANN library[2].

$$E(o,\{e\}) = \sum_{t} \sum_{i\in\{x,y,z\}} \sum_{u\in N_i(t)} w_{t,i,u}(o_{t,i,u} - e_{t,i,u})^2 \quad (2)$$

$$w_{t,i} = ||o_{t,i} - e_{t,i}||^{r-2} \quad (3)$$

During the search phase a weight for each neighborhood is calculated, for this purpose the energy function is written as equation 2 and the weight is calculated as shown in equation 3. $N_i(t)$ represents the neighborhoods found in each dimension x, y, z and u is the texel in the neighborhood of t, this means that a texel in the object is affected by multiple texels from different neighborhoods in the exemplar texture. The search is performed for every two texels $g_x = \{(i, 2*j, 2*k), \forall i,j,k\}$, g_x is the voxel in a slice perpendicular to x. This is done similarly for y and z, as shown in figure 1. We set $r = 0.8$ to perform a robust optimization [**?**]. Once the search phase is done the optimization phase takes place and it consists in averaging all the values found for each texel of the volume.

2.1.2. Optimization phase

The optimization phase consists in averaging the values that affect one texel in the object. Note that if the search phase is performed for every two texels as in 2.1.1, then the average will be for at most 75 texels (25 for each dimension).

$$o_t = \frac{\sum_{i\in\{x,y,z\}} \sum_{u\in N_i(t)} w_{u,i,t} * e_{u,i,t}}{\sum_{i\in\{x,y,z\}} \sum_{u\in N_i(t)} w_{u,i,t}} \quad (4)$$

Equation 4 shows the value of a texel in the object. When the texels present a high variability, the resulting object might be blurred, in order to avoid this, clustering is performed to only average those texels that correspond to the principal cluster. Following the optimization phase, the histogram matching is done to preserve the global statistics of the object relative to the exemplar.

2.1.3. Histogram Matching

To perform histogram matching, the CDF (cumulative distribution function) is calculated for both the exemplar and the object. Two $LUTs$ are constructed in order to perform faster calculations. The lookup table LUT_o maps the grey level value of the object to its corresponding value in the CDF_o, the lookup table LUT_e maps the CDF_e to the corresponding grey level value from the sample. The object is then modified by taking each of the texels t, using $LUT_o(t)$ to find the $CDF_o(t)$ and then using $LUT_e(CDF_o(t))$ to find the corresponding grey level value from the sample. The value of the object is then replaced by the corresponding value of the sample.

3. RESULTS AND EVALUATION

We test our method to synthesize virtual MR images and virtual $SR\mu CT$images of trabecular bone (see Figure 2(a)). The reference images were acquired for the needs of a study on osteoporosis, a disease inducing bone mass reduction and bone structure deterioration [**?**]. We have at our disposal a set of twelve 3D high resolution MR images with a cubic voxel of

[1] L. Smith 2002, A Tutorial on Principal Components Analysis; `www.cs.otago.ac.nz/cosc453/student_tutorials/principal_components.pdf`

[2] ANN: A library for approximate nearest neighbor searching; `http://www.cs.umd.edu/~mount/ANN/` Mount, D. M. and Arya, S. 2006

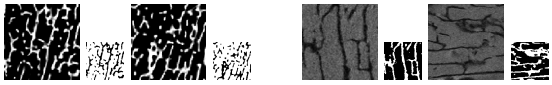

(a) 2D reference textures extracted from real images and binary masks.

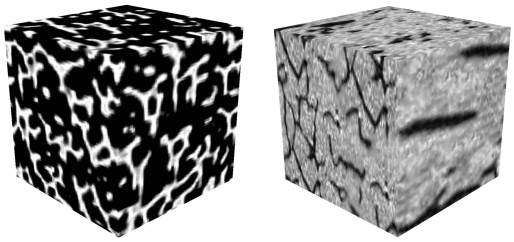

(b) 3D virtual images.

Fig. 2. Results of synthesis for $SR\mu CT$ (left) and μMRI (right) using multiple textures to constrain plans perpendicular to axis-directions and binary masks to enhance the untextured areas.

side 78μm and a set of twelve 3D $SR\mu CT$images downsampled to a resolution of 80μm to be on a comparable scale. As the MR images represent the marrow content of the samples, the contrast is inverted compared to $SR\mu CT$. We generated 3D virtual SRμCT and μMR images (128x18x128 voxels) from two random reference slices (83x83 pixels) extracted from a volume taken out of the SRμCT and μMR sets (Figure 2(a)).

We assess the accuracy of the virtual images from a statistical and a morphological point of view. As the ultimate goal is to produce synthetic images as close as possible to the reference ones, we compare their grey level distributions and some morphological bone parameters computed from their content. In this study, we only evaluate the quality of virtual μMR images (3D texture generated from SRμCT images has already been validated in [**?**]).

3.1. STATISTICAL ASSESSMENT

Figure 3 shows the histograms of the exemplar texture and the synthetic 3D μMR image shown in Figure 2. Note that when a randomly chosen slice is taken from the synthetic volume, the values of the histogram will be close to those of the exemplar, therefore, global statistics are still preserved. Thanks to the histogram matching, the grey levels distribution of the marrow and the bone are quite similar in the virtual image and the reference image. The statistics displayed near each histogram (mean, standard deviation, mode) are also very close.

3.2. MORPHOLOGICAL ASSESSMENT

In this part, we quantitatively compare some structural parameters of bone architecture obtained from the real and the

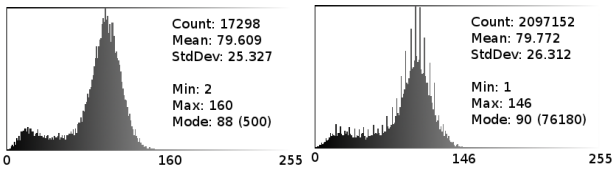

(a) 2D sample (b) 3D synthetic image

Fig. 3. Comparison of the histograms obtained from the reference 2D and the 3D synthetic μMR image.

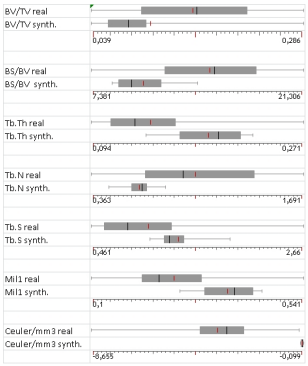

Fig. 4. Boxplots of morphological and topological bone parameters computed from real and synthetic μMR images.

synthetized μMR images. As displayed in Figure 3, the bone and marrow distribution are clearly overlapping, thus making the segmentation difficult. A more sophisticated method than a simple thresholding must be used to extract the trabecular bone. The same segmentation method was applied on the real and the virtual images [**?**]. This step is essential for the computation of the bone parameters.

We computed 3D morphological and topological architecture parameters from a set of twelve real μMR images and from a set of ten virtual μMR images. A 3D MIL (Mean Intercept Length) method was chosen to produce parameters related to the trabecular bone morphology and the Euler number was computed to estimate the bone topology. We considered the seven following parameters: Partial Bone Volume (BV/TV), Bone Surface to Bone Volume ratio (BS/BV), Trabecular Thickness (Tb. Th), Trabecular Number (Tb. N), Trabecular Separation (Tb. Sp)and Mean Intercept Length (MIL1). The connectivity was estimated by the Euler number (Euler/mm3)normalized by the total volume. The higher the Euler number's value, the less connected the bone structure is.

We assess the accuracy of the virtual images by comparing the bone parameters computed from the set of μMR images with those computed from synthetic ones. Figure 4 displays the boxplots associated to each bone parameter obtained from the sets of real and virtual μMR images. For the chosen representation, whiskers ends at minimum and maximum values, box starts at Q1 (first quartile) and ends at Q3 (third quar-

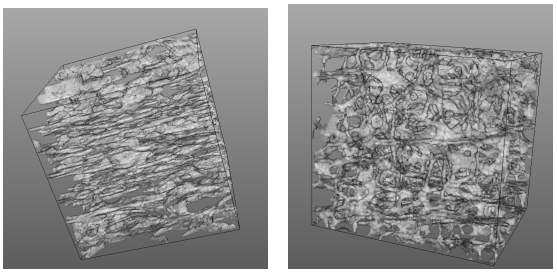

(a) Synthetic volume. (b) Original volume.

Fig. 5. Surface rendering of trabecular bone architecture obtained with: a) virtual μMR image, b) real μMR image.

tile), median appears in black, average in red. The scale line above the boxplots show the range of values of each parameter. It can be noticed that for all the morphologic parameters the distributions of the parameters computed from the virtual images are included in the range of values of those computed from the real images, thus proving the resemblance of the virtual bone with the real bone. They are also less spread, so the variability of the generated bone structures is reduced compared to the real set. Another set of randomly chosen reference slices would yield different results. For the topologic parameter (Euler/mm3), the score is slightly higher than the maximum value obtained with the μMR set, which remains satisfying. It means that the bone structure in the virtual images has a somewhat lower connectivity than in the reference set.

In Figure 5, segmented trabecular bones from the 3D virtual μMR images are compared to those obtained from the 3D μMR image from which were taken the reference slices for the texture synthesis. We retrieve visually the similarity demonstrated by the bone parameters.

4. CONCLUSION

Our method allows to create realistic 3D μMR and SRμCT images. We demonstrated quantitatively the accuracy of the synthetic texture from both statistical and morphological points of view. In future work, we will integrate our method into VIP (virtual imaging platform)[3], and we will continue towards the improvement of image simulation by providing realistic digital models to the platform.

5. REFERENCES

[1] C. Revol-Muller, H. Benoit-Cattin, Y. Carillon, C. Odet, A. Briguet, and F. Peyrin, "Bone mri segmentation assessment based on synchrotron radiation computed microtomography," *IEEE Trans Nucl Sci*, vol. 49, no. 1, pp. 220–224, 2002.

[2] D. Charpigny, T. Grenier, C. Odet, and H. Benoit-Cattin, "Towards iron oxide nanoparticles quantization in molecular mr images by default field deconvolution," in *Proc. ISBI 2009: 6th IEEE international symposium on biomedical imaging*, 2009.

[3] C. Castella, K. Kinkel, F. Descombes, M.P. Eckstein, P.E. Sottas, F.R. Verdun, and F.O. Bochud, "Mammographic texture synthesis: second-generationclustered lumpy backgrounds using agenetic algorithm," *Opt. Express*, vol. 16, no. 11, pp. 7595–7607, May 2008.

[4] Y. Holdstein, A. Fischer, L Podshivalov, and P.Z. XBar-Yoseph, "Volumetric texture synthesis of bone microstructure as a base for scaffold design," in *Shape Modeling International*, 2009, pp. 81–88.

[5] Johannes Kopf, Chi-Wing Fu, Daniel Cohen-Or, Oliver Deussen, Dani Lischinski, and Tien-Tsin Wong, "Solid texture synthesis from 2d exemplars," *ACM Transactions on Graphics (Proceedings of SIGGRAPH 2007)*, vol. 26, no. 3, pp. 2:1–2:9, 2007.

[6] C . Kwatra, I. Essa, A. Bobick, and N. Kwatra, "Texture optimization for example-based synthesis," *ACM Transactions on Graphics, SIGGRAPH 2005*, August 2005.

[7] S. Lefebvre and H. Hoppe, "Appearance-space texture synthesis," *ACM Trans. Graph.*, vol. 25, pp. 541–548, July 2006.

[8] J. P. Rolland, V. Vo, B. Bloss, and C. K. Abbey, "Fast algorithms for histogram matching: application to texture synthesis," *Journal of Electronic Imaging*, vol. 9, pp. 39–45, Jan. 2000.

[9] J.C. Prieto, C. Revol-Muller, F. Peyrin, P. Camelliti, and C. Odet, "3d texture synthesis for modeling realistic organic tissues," in *VISAPP'12 International Conference on Computer Vision Theory and Applications*, 2012, p. in press.

[10] C. Revol-Muller, F. Peyrin, Y. Carrillon, and C. Odet, "Automated 3d region growing algorithm based on an assessment function," *Pattern Recognition Letters*, 2002.

[3] http://www.creatis.insa-lyon.fr/vip/